Chemical Science
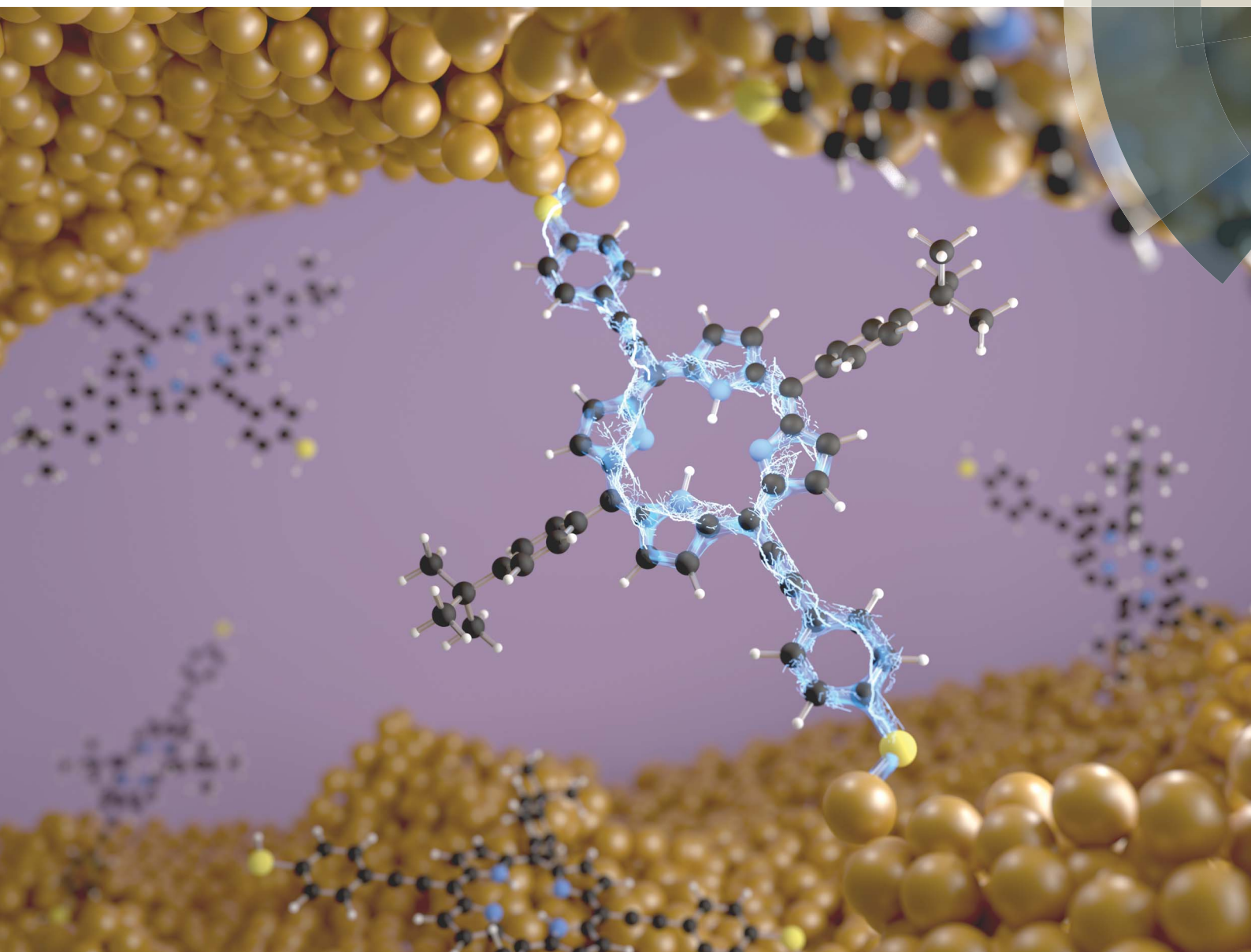
rsc.li/chemical-science

ROYAL SOCIETY
OF CHEMISTRY | Celebrating
IYPT 2019

EDGE ARTICLE
Marcel Mayor, Herre S. J. van der Zant, Diana Dulić *et al.*
Unravelling the conductance path through single-porphyrin
junctions

Check for updates

Unravelling the conductance path through single-porphyrin junctions†

Maria El Abbassi, [ID] ‡[a] Patrick Zwick,‡[b] Alfredo Rates,[ac] Davide Stefani, [ID] [a] Alessandro Prescimone, [ID] [b] Marcel Mayor, [ID] *[bde] Herre S. J. van der Zant [ID] *[a] and Diana Dulić [ID] *[c]

Porphyrin derivatives are key components in natural machinery enabling us to store sunlight as chemical energy. In spite of their prominent role in cascades separating electrical charges and their potential as sensitizers in molecular devices, reports concerning their electronic transport characteristics are inconsistent. Here we report a systematic investigation of electronic transport paths through single porphyrin junctions. The transport through seven structurally related porphyrin derivatives was repeatedly measured in an automatized mechanically controlled break-junction set-up and the recorded data were analyzed by an unsupervised clustering algorithm. The correlation between the appearances of similar clusters in particular sub-sets of the porphyrins with a common structural motif allowed us to assign the corresponding current path. The small series of model porphyrins allowed us to identify and distinguish three different electronic paths covering more than four orders of magnitude in conductance.

1   Introduction

Porphyrins and their related macrocycles are promising building blocks for the construction of functional molecular devices, as their rich and tunable optical and electrical properties can be employed in a wide range of applications, including those in catalysis, electrocatalysis, solar energy conversion, and photodynamic cancer therapy.[1–6] Furthermore, porphyrin synthesis is well established, allowing us to fine tune their chemical design in order to study fundamental charge transport through single molecules.[7–9] Side groups can be added to porphyrins in a modular way, allowing us to methodically test various chemical designs with different anchoring, bulky and spacer groups.[10] Additionally, expanded porphyrins have been suggested as building blocks for electronic applications displaying rich transport variety depending on their topology.[11]

However, it has been reported that porphyrin molecules have a low conductance value of the order of 1×10^{-5} G_0, albeit with a low β-attenuation factor especially at higher bias voltages,[12,13] with only a few studies recording higher conductance ($\approx 1 \times 10^{-4}$ G_0).[14,15] The extensive π-system enables the formation of molecular junctions with different stable configurations, leading to a large spread in conductance.[16,17] Studies about the influence of a coordinating metal show that the presence of a central ion hardly alters the conductance of the parent porphyrin structure.[18] However, the incorporation of Zn can induce conformational changes that lead to the appearance of an additional conducting state.[18] This rich variety of structural aspects reflected in their transport behaviour makes porphyrins interesting model compounds, but limits their potential for applications. These limitations could be overcome by an optimization of the molecular design, however the identification and characterization of the possible conductance paths at the single molecule level is required for this.

In this study, we systematically investigate transport across porphyrin-based compounds in order to identify the influence of structural features. In particular, the presence of anchoring groups, the bulkiness of the substituents, the presence of a metal ion and the dimension of the π-system are correlated with the recorded transport properties. For this reason, we synthesized seven different compounds with closely related geometry features, and measured them using an automatized mechanically controlled break-junction technique (MCBJ). By employing an unsupervised clustering algorithm[19,20] on a unique set of data consisting of almost 100 000 conductance traces, we identify classes of common behaviours in the

[a]Kavli Institute of Nanoscience, Delft University of Technology, 2600 GA Delft, The Netherlands. E-mail: h.s.j.vanderzant@tudelft.nl

[b]Department of Chemistry, University of Basel, CH-4056 Basel, Switzerland. E-mail: marcel.mayor@unibas.ch

[c]Department of Physics, Department of Electrical Engineering, Faculty of Physical and Mathematical Sciences, University of Chile, Avenida Blanco Encalada 2008, Santiago 8330015, Chile. E-mail: ddulic@ing.uchile.cl

[d]Institute of Nanotechnology (INT), Karlsruhe Institute of Technology (KIT), D-76021 Karlsruhe, Germany

[e]Lehn Institute of Functional Materials (LIFM), School of Chemistry, Sun Yat-Sen University (SYSU), Guangzhou 510275, China

‡ These authors contributed equally to this work.

breaking traces and their correlation with structural features of the molecules under investigation enables us to link each of them to a different electron pathway across the porphyrins.

2 Experimental

The chemical structure of the porphyrin molecules included in this study can be found in Fig. 1a and b. Compounds **P1**, **P2** and **P3** share the same linear backbone, consisting of the porphyrin core, phenylene–acetylene spacers and thiol anchoring groups, but vary in their lateral bulky groups. With this series, the influence of the steric requirement of the peripheral phenyl subunit shall be studied. **ZnP1**, a variant of **P1** which includes a Zn(ɪɪ) ion in the porphyrin core, is employed to investigate variations in the transport characteristics emerging from the presence of the metal center.

The role of the anchoring groups and of the spacers is investigated by comparing the results of **P1** with those obtained from three derivatives that possess the same lateral bulky groups, but have different components in their backbones (Fig. 1b): **R1** exposes only on one side the backbone structure of **P1** comprising a thiol anchor group, **R2** has neither acetylene spacers nor anchoring groups, whereas **R3** has a similar backbone to **P1**, but with terminal *tert*-butyl groups replacing the thiol anchoring groups.

Samples consist of a thin gold constriction suspended on top of a flexible substrate coated with an insulating layer of polyimide, as depicted in Fig. 1c. The sample is mounted in a three-point bending mechanism, clamped between two lateral supports and the head of a central pushing rod. Upon bending, the gold wire stretches until rupture, which leaves two atomically sharp electrodes whose separation can be adjusted mechanically. The wire can be fused back by reducing the deformation of the substrate. The breaking–making process can be repeated thousands of times while the conductance of the junction is recorded. A two-dimensional (2D) histogram of the conductance *vs.* displacement is built from the "breaking traces". The measurements were performed in an MCBJ setup at room temperature in air. All the measurements presented in this work have been performed with a bias voltage of 100 mV. Each dataset presented in this work consists of 10 000 consecutive traces recorded on the same junction and without data selection.

3 Synthesis

The porphyrin model compounds studied in this work were synthesised by variations of reported procedures, which are summarized in Fig. 2.[21,22] The porphyrin subunits of **R2** and the intermediates **1**, **2**, and **3** were assembled from the corresponding bis-pyrroles and aldehydes. For the precursor **7** of the mono-functionalized porphyrin, both aldehydes were used in equal amounts. Condensation of literature-known 2,2′-((4-(*tert*-butyl)phenyl)methylene)bis(1*H*-pyrrole)[23] with either 4-(*tert*-butyl)benzaldehyde or commercially available 3-(trimethylsilyl)propiolaldehyde provided **R2** or **1** respectively. Using instead either 2,2′-((3,5-di-*tert*-butylphenyl)methylene)bis(1*H*-pyrrole)[24]
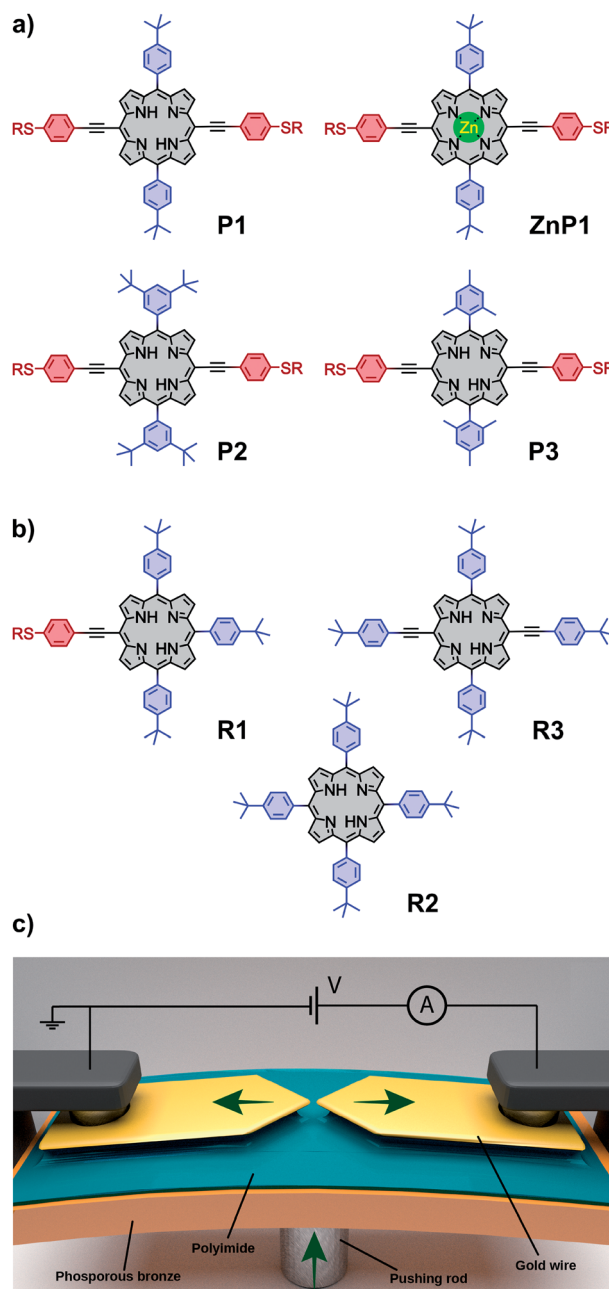

Fig. 1 (a) Structural designs of **P1**, **ZnP1**, **P2** and **P3**; (b) structural formula of **R1**, **R2** and **R3**. The different parts of the molecule have been coloured dividing the anchoring groups (red) and the bulky side groups (blue). The molecules are synthesized with R = acetyl, but upon deprotection at the electrode surface, R represents either a hydrogen atom or the gold electrode. (c) Schematics of the mechanically controllable break-junction (MCBJ) setup.

or 2,2′-(mesitylmethylene)bis(1*H*-pyrrole)[21] in combination with 3-(trimethylsilyl)propiolaldehyde provided **2** and **3** respectively. The less symmetric **7** was condensed from a 2/1/1 mixture of 2,2′-((4-(*tert*-butyl)phenyl)methylene)bis(1*H*-pyrrole),[23] 4-(*tert*-butyl)benzaldehyde, and 3-(triisopropylsilyl)propiolaldehyde.[25] For the condensation reactions, a protocol of Anderson *et al.* was adapted, which was already used for the preparation of literature-known **2**.[26]
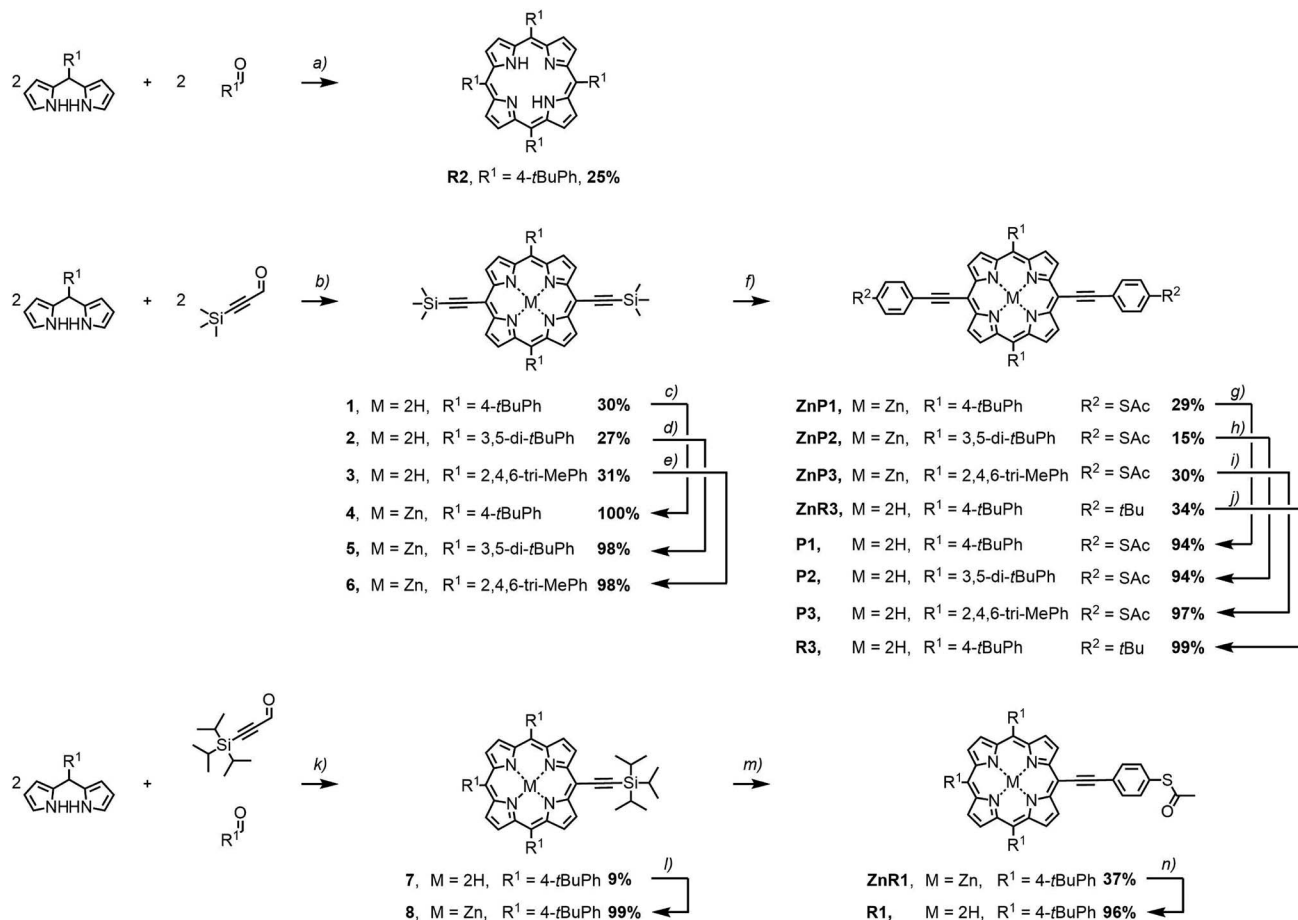
Fig. 2 Synthetic overview. (a) (1) $BF_3 \cdot OEt_2$, CH_2Cl_2, rt, 45 min. (2) DDQ, CH_2Cl_2, rt, 1 h. (b) (1) $BF_3 \cdot OEt_2$, CH_2Cl_2, 0 °C rt, 5 20 min. (2) DDQ, CH_2Cl_2, rt, 1 h. (c–e) $Zn(OAc)_2$, CH_2Cl_2, CH_3OH, rt, 1 h to 3 d. (f) (1) TBAF, 2Me-THF, rt, 1 h. (2) S-(4-Iodophenyl)ethanethioate, $Pd(PPh_3)_4$, CuI, THF, NEt_3, rt, 1–16 h. (g–j) TFA, CH_2Cl_2, rt, 2 h. (k) (1) $BF_3 \cdot OEt_2$, CH_2Cl_2, rt, 5 min. (2) DDQ, CH_2Cl_2, rt, 1 h. (l) $Zn(OAc)_2$, CH_2Cl_2, CH_3OH, rt, 1 h. (m) (1) TBAF, 2Me-THF, rt, 1 h. (2) S-(4-Iodophenyl)ethanethioate, $Pd(PPh_3)_4$, CuI, THF, NEt_3, rt, 16 h. (n) TFA, CH_2Cl_2, rt, 2 h.

Condensation reactions were catalysed by $BF_3 \cdot OEt_2$ in CH_2Cl_2 at either 0 °C or room temperature for 5 to 45 minutes prior to oxidation by 2,3-dichloro-5,6-dicyano-p-benzoquinone (DDQ) at room temperature for one hour. The c_2 symmetric porphyrins **R2**, **1**, **2** and **3** were isolated in typical yields of 27 to 31%. The less symmetric compound **7** was condensed in a statistic fashion leading to 9% yield. Metalation of the porphyrins by zinc(II) acetate in a CH_2Cl_2/CH_3OH mixture for one hour to three days at room temperature provided the Zn–porphyrins **4**, **5**, **6**, and **8** almost quantitatively.

Further functionalization of the porphyrins **4–6** required the liberation of the alkyne group, which was achieved by treatment with tetrabutylammonium fluoride (TBAF) at room temperature for one hour in 2-methyltetrahydrofuran (2Me-THF). Without further purification, these compounds were engaged in Sonogashira–Hagihara cross couplings[22] with excesses of the iodoaryls of interest. The coupling reaction was performed in dry and degassed THF and NEt_3 with $Pd(PPh_3)_4$ and CuI as catalysts at room temperature with reaction periods between 2 and 16 hours. Using S-(4-iodophenyl)ethanethioate as iodoaryl gave access to **ZnP1** in isolated yields of 29%. Treatment with trifluoroacetic acid (TFA) in CH_2Cl_2 for two hours at room

temperature gave the free base analogues **P1**, **P2**, **P3**, **R1**, and **R3** almost quantitatively.

The identity of all porphyrin derivatives was corroborated by ^{1}H-NMR spectroscopy and mass spectrometry. In addition, single crystals suitable to analyse the solid state structure by X-ray diffraction were obtained for **1**, **2**, **3**, **4**, **5**, **ZnP1**, **P2**, and **R2**. A sulphur-to-sulphur distance of 2.41 nm could be extracted from the crystallographic data of **ZnP1** and **P2**, showing independence of the structural variations, such as bulky groups or the incorporated Zn(II) ion (Fig. 3). Detailed description of the experimental procedures and the analytical data of all the compounds are provided as ESI.†

4 Results

Fig. 4a and b show the 2D histograms of two representative measurements performed on **P1** and **R2**, respectively. While for **P1** a clear plateau is found above 1×10^{-4} G_0 and extending for about 2 nm (Fig. 4a), no clear plateau is observed in the case of **R2**. Examples of individual breaking traces recorded for each molecule are presented in Fig. 4c and d. Clear and flat plateaus above 1×10^{-4} G_0 are observed in the case of **P1**, whereas, in the case of **R2**, the plateau is absent. All the molecules containing
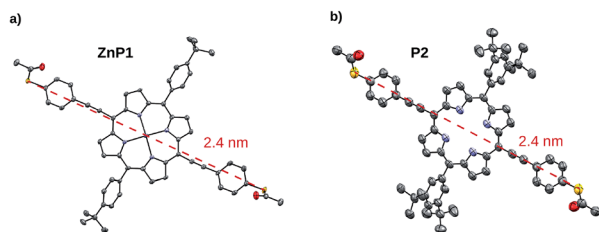
Fig. 3 ORTEP-representation of solid-state structures. (a) **P2** and (b) **ZnP1**. Thermal ellipsoids are plotted at a 50% probability level. The dashed red line displays the main axis and the S–S distance.

two thiol groups as anchoring sites (**P1, P2, P3, ZnP1**) show a similar conductance histogram to that in Fig. 4a with a very well-defined plateau, in contrast to the measurements of the reference molecules **R1, R2** and **R3** which lack this design feature (see Fig. S1†).

To further investigate the charge transport pathways, an unsupervised clustering algorithm has been used to subdivide the different datasets in four different classes.[20] Classes A–C are associated with the presence of a molecule inside the junction, whereas class D (see Fig. S2†) contains the traces in which no molecular junction has been formed and only shows the exponential decay typical of tunnelling that occurs through a barrier. The results obtained for **P1** are reported in Fig. 5, as an example. Class A constitutes 64.7% of the molecular junctions and
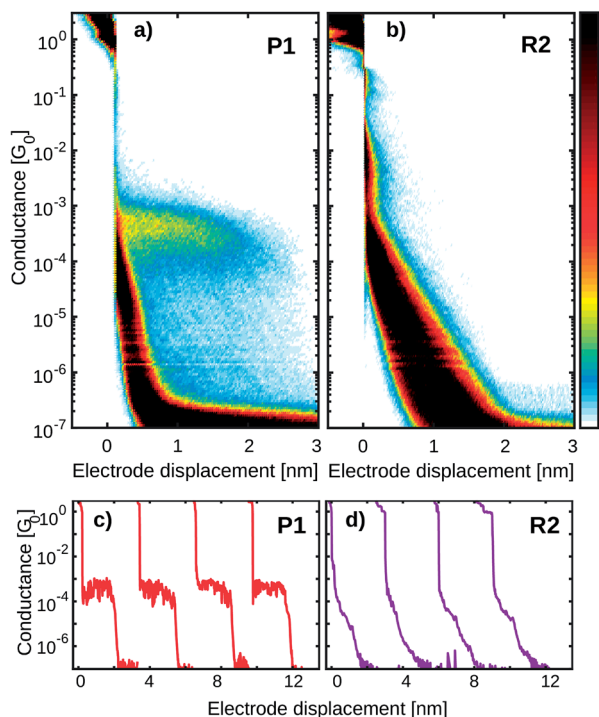
contains the traces that exhibit a plateau of about 2.2 nm length. A log-normal fit to the peak in the 1D conductance histogram reveals it being centred around 2×10^{-4} G_0 (red colored high-conductance area in Fig. 5c). The traces grouped in class B (28.8%) form a slightly shorter and wider plateau, centred at 3×10^{-5} G_0 (green colored medium-conductance class in Fig. 5c). Finally, class C (6.5%) shows a broad feature centred at 2×10^{-6} G_0 (blue in Fig. 5d). The three classes together constitute 12.6% of the total traces. The same clustering analysis has been applied to all the datasets and four groups with similar features have been found. Table 1 summarizes the occurrence of each class for the various molecules.
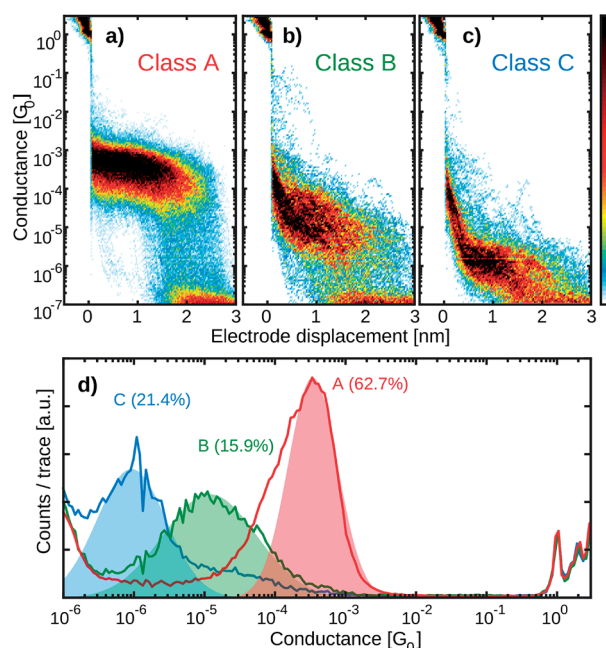

Fig. 5 Clustering analysis of the conductance properties of **P1**. (a–c) Two-dimensional histograms of the three different categories of breaking traces obtained from the reference-free cluster analysis applied to **P1**. (d) One-dimensional conductance histograms corresponding to classes A, B and C. By fitting a log-normal distribution to the one-dimensional histograms, we can extract the conductance peak positions at 2×10^{-4} G_0 for class A (64.7% of the molecular traces), 3×10^{-5} G_0 for class B (28.8%) and 2×10^{-6} G_0 in the case of class C (6.5%).

Fig. 4 Two-dimensional conductance *vs.* displacement histograms built from 10 000 consecutive breaking traces of (a) **P1** and (b) **R2**; no data selection was made. Both measurements were performed with a bias of 100 mV at room temperature. Examples of individual conductance breaking traces for (c) **P1** and (d) **R2** (with a horizontal offset of 3 nm for clarity).

Table 1 Summary of the occurrence of the three molecular classes for each molecule. Class A corresponds to the high-conductance class, class B corresponds to the medium-conductance class and class C corresponds to the low-conductance class

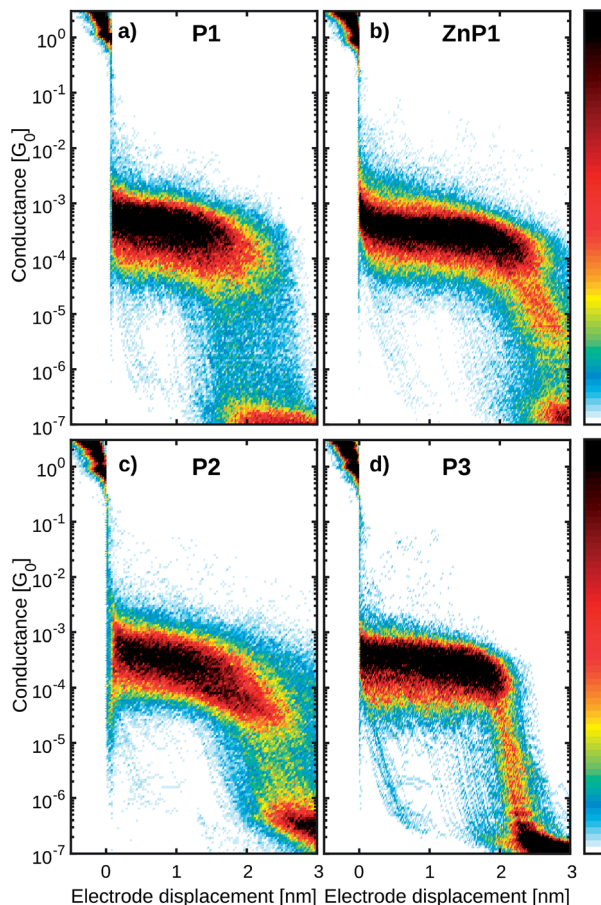| Molecule	Class A	Class B	Class C
P1	✓	✓	✓
P2	✓	✓	✓
P3	✓	✓	✓
ZnP1	✓	✓	✓
R1			✓
R2			
R3		✓	✓

Fig. 6 Two-dimensional conductance *vs.* displacement histograms for (a) **P1**, (b) **ZnP1**, (c) **P2** and (d) **P3**. The histograms only include breaking traces with the behaviour present in class A. All datasets have similar length and conductance values.

5 Discussion

While class A is present only in the four compounds containing two thiol anchoring groups (**P1**, **P2**, **P3** and **ZnP1**), class B is also found in **R3**. Class C, on the other hand, is present in all the measurements except those of **R2**. The 2D conductance histograms of class A obtained in the case of the molecules containing the same backbone exposing two terminal thiol groups (**P1**, **ZnP1**, **P2** and **P3**) are displayed in Fig. 6. The observed differences in plateau conductance or length are within the variations typically found in MCBJ experiments even when performed on the same molecule.[27] For this reason, we attribute this feature to the junction configuration in which the molecule is connected to both electrodes *via* the thiols and transport occurs from sulfur to sulfur. This is supported by the average trace length of about 2 nm, which is in good agreement with the estimated length from the crystallographic measurements of the sulfur-to-sulfur distance (Fig. 3). Noticeably, the presence of the Zn atom does not affect this plateau, indicating that the electron paths involved in transport are mainly localized on the aromatic system of the ligand.[12] We further note that for **P3**, class A exhibits the least slanted conductance plateau with the narrowest distribution (see Table S1†). In addition, the breaking of the molecular junction around 2 nm occurs in a more abrupt way compared to the other derivatives. In this respect, it is interesting that the bulky groups of **P3** are more spatially localized above and below the porphyrin system than for the other molecules **P1** and **P2**, thus reducing access to the π system of the porphyrin core.

The correlation of the presence/absence of particular classes with the structure of the studied porphyrin allows us to assign possible transport paths of the molecular junction (Fig. 7 and S17†). Class A is assigned to the molecule bridging the electrodes *via* the thiol anchor groups, as intended by the molecular design (Fig. 7a). The matching length of the plateau with the dimension of the structure and the fact that exclusively the porphyrins with terminal thiol-exposing backbones show that this class corroborate the assignment.

Both classes B and C are not observed for the porphyrin compound without phenylene–acetylene spacers (**R2**), suggesting that their presence introduces additional charge transport pathways. Compared to that observed in class A, the plateau in class B has a lower conductance, and it is shorter, more spread out and observed less frequently. In the case of **R3**, not containing any thiol groups, this plateau is more slanted. Hence, the presence of the thiol groups seems to stabilize the junction, yielding more defined plateaus even if the electron injection does not occur through the sulfur atom. The charge transport pathway could thus involve the acetylene spacer or the phenyl
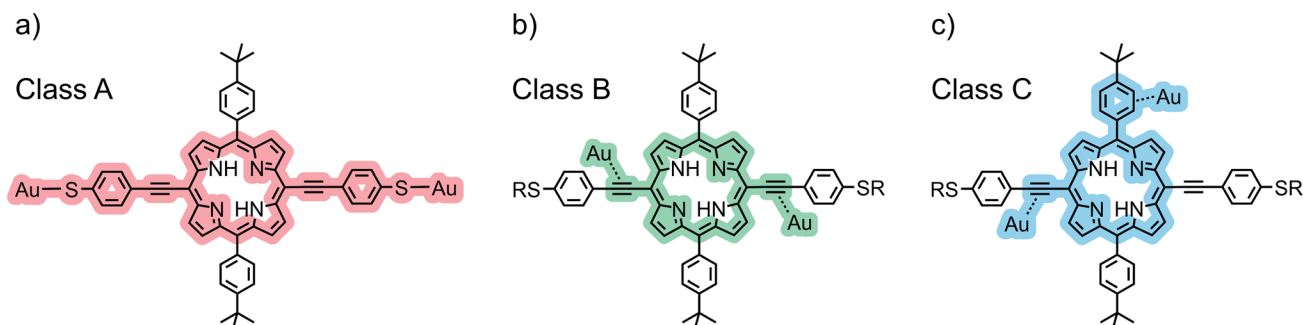

Fig. 7 Suggested transport pathways corresponding to the 3 different classes through the molecular structure displayed with **P1**. Au represents the electrode. The contact to the corresponding subunit is schematically drawn.

ring on both sides of the molecule, as it is not observed in molecules that do not contain these groups (Fig. 7b).

Class C, on the other hand, can be related to the path that results from injection in the π-system of the acetylene group and ends at one of the lateral phenyl rings (Fig. 7c). This is suggested by the fact that this class is also observed in molecule **R3** that does not have sulfur atoms in its structure but comprises the components suggested for the current path. In this case, however, the plateau is more slanted, again suggesting that the sulfur plays a role in the stability of the junction configuration. The role of sulfur in mechanically stabilizing the junction configuration is also corroborated by the reduced conductance spread in **R1**, which does expose a thiol as a potential mechanical anchor, compared to **R2** and **R3**, which do not. To check the stability of the different classes, self-breaking measurements were performed in the case of compound **P1** (see Fig. S6† for more details). While class A showed high stability (up to 5 minutes at room temperature), the lifetime of classes B and C did not exceed the tens of seconds. These observations confirm the hypothesis about the mechanical stabilization role of the thiol anchors.

The pathways attributed to classes B and C can be compared to the "*para*" and "*ortho*" paths found by Li *et al.* in the case of porphyrins without acetylene spacers and with pyridine anchoring groups.[15] While in their experiments the two pathways resulted in conductances that differed by a factor of 1.4, in our case the difference is about an order of magnitude.

Finally, apart from tunnelling traces (class D), none of the classes found in **R2** exhibits a clear molecular signature. This confirms that the bulky groups do not form an efficient injection point for charges and that the transport path from one bulky group to another is ineffective.

6 Conclusion

In this study, we report an unprecedented dataset of almost 300 000 traces measured on seven different porphyrin derivatives. We identified transport pathways by methodically and purposefully modifying the chemical design of these porphyrin-based compounds and by applying an unbiased clustering algorithm for the analysis of the breaking traces. By introducing phenylene–acetylene as the spacer and thiols as anchor groups, we achieved very stable molecular junctions with a high conductance up to 2×10^{-4} G_0. The observed high-conductance plateau is related to the thiol-to-thiol conduction path. Both, bulky groups and the Zn ion as a metal center did not have a significant influence on the junction properties, suggesting that the conductance through the molecule is mainly localized on the conjugated porphyrin system. Other classes with lower conductance were found and were related to the presence of phenylene–acetylene spacers.

Conflicts of interest

There are no conflicts to declare.

Acknowledgements

Notes and references

1 T. S. Balaban, Tailoring porphyrins and chlorins for self-assembly in biomimetic artificial antenna systems, *Acc. Chem. Res.*, 2005, **38**(8), 612–623.

2 S. Horn, K. Dahms and M. O. Senge, Synthetic transformations of porphyrins–advances 2004-2007, *J. Porphyrins Phthalocyanines*, 2008, **12**(10), 1053–1077.

3 M. Jurow, A. E. Schuckman, J. D. Batteas and C. Michael Drain, Porphyrins as molecular electronic components of functional devices, *Coord. Chem. Rev.*, 2010, **254**(19–20), 2297–2310.

4 T. D. Lash, K. M. Kadish, K. M. Smith, and R. Guilard, *The porphyrin handbook*, ed. K. M. Kadish, 2000, pp. 125–200.

5 Z. Liu, A. A. Yasseri, J. S. Lindsey and D. F. Bocian, Molecular memories that survive silicon device processing and real-world operation, *Science*, 2003, **302**(5650), 1543–1545.

6 M. L. Perrin, C. J. O. Verzijl, C. A. Martin, A. J. Shaikh, R. Eelkema, J. H. Van Esch, J. M. Van Ruitenbeek, J. M. Thijssen, H. S. J. van der Zant and D. Dulić, Large tunable image-charge effects in single-molecule junctions, *Nat. Nanotechnol.*, 2013, **8**(4), 282.

7 T. Tanaka and A. Osuka, Conjugated porphyrin arrays: synthesis, properties and applications for functional materials, *Chem. Soc. Rev.*, 2015, **44**(4), 943–969.

8 F. Moresco, G. Meyer, K.-H. Rieder, H. Tang, A. Gourdon and C. Joachim, Conformational changes of single molecules induced by scanning tunneling microscopy manipulation: A route to molecular switching, *Phys. Rev. Lett.*, 2001, **86**(4), 672.

9 O. Shoji, H. Tanaka, T. Kawai and Y. Kobuke, Single molecule visualization of coordination-assembled porphyrin macrocycles reinforced with covalent linkings, *J. Am. Chem. Soc.*, 2005, **127**(24), 8598–8599.

10 Z. Li, M. Smeu, M. A. Ratner and E. Borguet, Effect of anchoring groups on single molecule charge transport through porphyrins, *J. Phys. Chem. C*, 2013, **117**(29), 14890–14898.

11 T. Stuyver, M. Perrin, P. Geerlings, F. De Proft and M. Alonso, Conductance switching in expanded porphyrins through aromaticity and topology changes, *J. Am. Chem. Soc.*, 2018, **140**(4), 1313–1326.

12 E. Leary, B. Limburg, A. Alanazy, S. Sangtarash, I. Grace, K. Swada, L. J. Esdaile, M. Noori, M. Teresa González, G. Rubio-Bollinger, H. Sadeghi, A. Hodgson, N. Agraït, S. J. Higgins, C. J. Lambert, H. L. Anderson and

R. J. Nichols, Bias-driven conductance increase with length in porphyrin tapes, *J. Am. Chem. Soc.*, 2018, **140**(40), 12877–12883.

13 G. Sedghi, V. M. García-Suárez, L. J. Esdaile, H. L. Anderson, C. J. Lambert, M. Santiago, D. Bethell, S. J. Higgins, M. Elliott, J. Neil Bennett, E. Macdonald and R. Nichols, Long-range electron tunnelling in oligo-porphyrin molecular wires, *Nat. Nanotechnol.*, 2011, **6**(8), 517.

14 G. Sedghi, K. Sawada, L. J. Esdaile, M. Hoffmann, H. L. Anderson, D. Bethell, W. Haiss, S. J. Higgins and R. J. Nichols, Single molecule conductance of porphyrin wires with ultralow attenuation, *J. Am. Chem. Soc.*, 2008, **130**(27), 8582–8583.

15 Z. Li and E. Borguet, Determining charge transport pathways through single porphyrin molecules using scanning tunneling microscopy break junctions, *J. Am. Chem. Soc.*, 2011, **134**(1), 63–66.

16 M. L. Perrin, F. Prins, C. A. Martin, A. J. Shaikh, R. Eelkema, J. H. van Esch, T. Briza, R. Kaplanek, V. Kral, J. M. van Ruitenbeek, S. Herre, J. van der Zant and D. Dulić, Influence of the chemical structure on the stability and conductance of porphyrin single-molecule junctions, *Angew. Chem., Int. Ed.*, 2011, **50**(47), 11223–11226.

17 M. L. Perrin, C. A. Martin, F. Prins, A. J. Shaikh, R. Eelkema, J. H. van Esch, J. M. van Ruitenbeek, S. Herre, J. van der Zant and D. Dulić, Charge transport in a zinc–porphyrin single-molecule junction, *Beilstein J. Nanotechnol.*, 2011, **2**(1), 714–719.

18 Z.-F. Liu, S. Wei, H. Yoon, O. Adak, I. Ponce, Y. Jiang, W.-D. Jang, L. M. Campos, L. Venkataraman and J. B. Neaton, Control of single-molecule junction conductance of porphyrins *via* a transition-metal center, *Nano Lett.*, 2014, **14**(9), 5365–5370.

19 M. Lemmer, M. S. Inkpen, K. Kornysheva, N. J. Long and T. Albrecht, Unsupervised vector-based classification of single-molecule charge transport data, *Nat. Commun.*, 2016, **7**, 12922.

20 D. Cabosart, M. El Abbassi, D. Stefani, R. Frisenda, M. Calame, S. Herre, J. van der Zant and M. L. Perrin, A reference-free clustering method for the analysis of molecular break-junction measurements, *Appl. Phys. Lett.*, 2019, **114**(14), 143102.

21 K. F. Cheng, C. Michael Drain and K. Grohmann, Porphyrins linked directly to the 5, 5′ positions of 2, 2′-bipyridine: A new supramolecular building block and switch, *Inorg. Chem.*, 2003, **42**(6), 2075–2083.

22 K. Sonogashira, T. Yasuo and N. Hagihara, A convenient synthesis of acetylenes: catalytic substitutions of acetylenic hydrogen with bromoalkenes, iodoarenes and bromopyridines, *Tetrahedron Lett.*, 1975, **16**(50), 4467–4470.

23 D. K. Dogutan, S. H. H. Zaidi, P. Thamyongkit and J. S. Lindsey, New route to abcd-porphyrins *via* bilanes, *J. Org. Chem.*, 2007, **72**(20), 7701–7714.

24 M. J. Plater, S. Aiken and B. Grant, Metallated porphyrins containing lead (ii), copper (ii) or zinc (ii), *Tetrahedron*, 2002, **58**(12), 2415–2422.

25 O. Robles and F. E. McDonald, Modular synthesis of the c9-c27 degradation product of aflastatin a *via* alkyne-epoxide cross-couplings, *Org. Lett.*, 2008, **10**(9), 1811–1814.

26 P. N. Taylor and H. L. Anderson, Cooperative self-assembly of double-strand conjugated porphyrin ladders, *J. Am. Chem. Soc.*, 1999, **121**(49), 11538–11545.

27 R. Frisenda, D. Stefani, S. Herre and J. van der Zant, Quantum transport through a single conjugated rigid molecule, a mechanical break junction study, *Acc. Chem. Res.*, 2018, **51**(6), 1359–1367.